Journal of Zhejiang University SCIENCE A
ISSN 1673-565X (Print); ISSN 1862-1775 (Online)
www.zju.edu.cn/jzus; www.springerlink.com
E-mail: jzus@zju.edu.cn

Focusing with the decomposition of the time reversal operator method in noisy environments*

Chun-xiao LI[1], Jian-long LI[†‡1], Xian-yi GONG[1,2], Ming-fei GUO[3]

([1]*Department of Information Science and Electronic Engineering, Zhejiang University, Hangzhou 310027, China*)

([2]*Hangzhou Applied Acoustics Research, Hangzhou 310012, China*)

([3]*MOE Key Laboratory of Mechanical Manufacture and Automation, Zhejiang University of Technology, Hangzhou 310014, China*)

[†]E-mail: JLLi@zju.edu.cn

Received July 14, 2008; Revision accepted Oct. 22, 2008; Crosschecked Apr. 27, 2009

Abstract: This paper presents a detailed analysis of the effects of noise (reverberation) on the focusing performance of decomposition of the time reversal operator (DORT) in a noise-limited case and in a reverberation-limited case, respectively. Quantitative results obtained from simulations and experiments are presented. The results show the DORT method can be efficiently applied to target detection with enough source level to yield significant backscatter. For a target placed on the bottom, the influence of the reverberation on the focusing performance is slight. However, distinguishing between a target and constant backscattering returning from strong local clutter on the bottom (false alarms) needs further research.

Key words: Decomposition of the time reversal operator (DORT), Time reversal mirror, Retrofocusing performance
doi:10.1631/jzus.A0820563 **Document code:** A **CLC number:** O42; TP391; P7

INTRODUCTION

A time reversal mirror has been demonstrated theoretically and experimentally in ocean acoustics, which can produce temporally and spatially focused acoustic signals at the original position of the probe source (Jackson and Dowling, 1991; Kuperman *et al*., 1998; Roux and Fink, 2000). The directivity of a time reversal array will suppress reverberation and will highlight strong acoustic scatterers, thereby improving the performance of the active sonar system (Jackson and Dowling, 1991). The enhancement of the echo-to-reverberation ratio by the method of time-reversal was also demonstrated experimentally in shallow water (Kim *et al*., 2004). However, a time reversal mirror is limited by the requirement that a probe source initially broadcasts signals from the desired focal position. In recent years, great efforts have been made to refocus at positions other than that of the probe source or refocus at any location without the need for a probe source. Using frequency shift or extracting isolated modes, a time reversal mirror can refocus at ranges or depths other than that of the probe source (Song *et al*., 1998; Walker *et al*., 2005). Moreover, a time reversal mirror can refocus at integer multiples of the iteration ranges using sampled response iteration in a range-independent shallow-ocean waveguide without a probe source (Walker *et al*., 2006).

The use of acoustic backscattered signals to detect and classify underwater targets has also attracted significant attention. The decomposition of the time reversal operator (DORT) applied to a point scatterer has been demonstrated (Prada *et al*., 1995; 1996; Carin *et al*., 2004; Gaumond *et al*., 2006). Moreover, Lingevitch *et al*.(2002) and Song *et al*.(2004; 2005) extended this method by using backscattering from a rough water-bottom interface as a surrogate probe

‡ Corresponding author

* Project supported by the National Natural Science Foundation of China (Nos. 60702022 and 60772094), and the National Basic Research Program (973) of China (No. 5132103ZZT21B)

source. However, most previous investigations on time reversal mirrors assumed that the input signal-to-noise ratio (SNR) of the array was high. For example, this technique was tested at sea using an echo repeater to simulate the target response (Song *et al*., 1999; Gaumond *et al*., 2006). Few papers emphasized how noise affected the performance of acoustic time reversal (Sabra *et al*., 2002; Folegot *et al*., 2003; Li C.X. *et al*., 2008). Folegot *et al*.(2003) studied the effects of bottom reverberation and absorption and showed a method to overcome them. Sabra *et al*.(2002) presented theoretical results that were limited to active focusing with a probe source. They concluded that noise influences a time reversal mirror with a probe source twice because not only will the source receive array (SRA) receive and then retransmit noise (when it receives the signal transmitted by the probe source) but also the intended signal may be masked by ambient noise at the retrofocus location. Similarly, noise also influences DORT twice. However, the effect of the noise (or the reverberation) on performance degradation is different. It is possible that the DORT is mainly influenced by reverberation which is not present in a time reversal mirror with a probe source. For DORT, although the SRA does not directly broadcast noise (or the reverberation) in the process of retransmitting the time-reversed signals, the transfer function vector used to weight the signals may be incorrectly estimated. Therefore, the reason that noise (or the reverberation) influences DORT in the process of retransmission is that it contaminates the time reversal operator. At the intended retrofocus location, the retransmitted signal is again contaminated by noise, as in the case of the time reversal mirror with a probe source. In this study, this aspect of noise is not considered.

In practice, it is difficult to guarantee a high signal-to-noise (reverberation) ratio when the received signal is the backscattering from a point scatterer, especially in a shallow water environment. This research reports the results of an analytical and simulation investigation on how noise influences the focusing performance of the DORT in shallow ocean environments. The results are then demonstrated by a laboratory waveguide experiment. Two cases are considered. One is a noise limited case in which the dominant impediment to reception of the echo is additive noise, and the other is a reverberation limited case in which the dominant impediment is bottom reverberation. The purpose of this study is to evaluate whether the DORT can be applied and how to use it in both cases.

THEORY

Time reversal operator in a noise-free case

The DORT method is a scattering analysis technique developed from the study of the iterative time reversal process. It can selectively focus on scatterers in a multi-target environment. A set of source elements transmit a sequence of signals and each receiver element records the signal resulting from each transmission. Assume that the array of the time reversal mirror consists of N elements and that the medium contains a single point-like scatterer with reflection coefficient $A(f)$. The DORT algorithm is based on the measurement of the response matrix $\boldsymbol{k}_{jl}(f)$, i.e., the backscattered field on channel j of the time reversal mirror due to an impulsive signal broadcast from channel l. Moreover, because the response matrix $\boldsymbol{k}_{jl}(f)$ of this element-to-element measurement makes it difficult to guarantee a high SNR, N orthogonal beams rather than the individual source array elements have been used to probe the waveguide (Lingevitch *et al*., 2002). Here, we still use the element-to-element measurement because the methods have no substantial distinction if different SNRs are assured for simulation purposes. For each frequency component, a transfer matrix is defined as $\boldsymbol{K}(f)$. The time reversal operator (TRO) is defined by $\boldsymbol{K}^{\boldsymbol{H}}(f)\boldsymbol{K}(f)$ where $\boldsymbol{H}$ denotes complex conjugation, and it is a Hermitian matrix. If we also assume a high echo-to-noise ratio excluding the noise component in the derivation, then $\boldsymbol{K}(f)$ can be expressed as (Gaumond *et al*., 2006)

$$\boldsymbol{K}(f)=\boldsymbol{G}(f)A(f)\boldsymbol{G}^{\mathrm{T}}(f), \tag{1}$$

where $\boldsymbol{G}(f)=[G(z_1,r_o,z_o,f)\ G(z_2,r_o,z_o,f)\ \ldots\ G(z_N,r_o,z_o,f)]^{\mathrm{T}}$ is the array transfer function vector (multichannel Green's function) between the scatterer and the time reversal mirror array, where r_o and z_o are the range and depth of the object (scatterer). The TRO can be decomposed in terms of the eigenvalues $\lambda_i(f)$ and eigenvectors $\boldsymbol{u}_i(f)$ as

$$\boldsymbol{K}^{\boldsymbol{H}}(f)\boldsymbol{K}(f)=\sum_{n=1}^{N}\lambda_i(f)\boldsymbol{u}_i(f)\boldsymbol{u}_i^*(f). \quad (2)$$

Since the TRO is a rank 1 matrix for a single scatterer, the first eigenvector $\boldsymbol{u}_1(f)$ is parallel and proportional to the transfer function vector $\boldsymbol{G}(f)$:

$$\boldsymbol{G}(f)=a\boldsymbol{u}_1(f), \quad (3)$$

where a is an arbitrary complex value. When the transfer function vector is normalized, $|a|=1$.

Hence, the estimate of the transfer vector is the first eigenvector $\hat{\boldsymbol{G}}(f)=\boldsymbol{u}_1(f)$. A retransmission with elements weighted by it will focus the energy onto the scatterer.

Signal plus noise case

If the noise cannot be ignored compared to the echo resulting from the transmitted signal $s(f)$, let $p(j,l,f)$, $1\leq j, l\leq N$ define the pressure that is received at the jth receiver with the lth source transmission:

$$p(j,l,f)=G(z_j,r_o,z_o,f)A(f)G(z_l,r_o,z_o,f)s(l,f)+N_{j,l}(f), \quad (4)$$

where $G(z_j,r_o,z_o,f)$ is the propagation function between the scatterer (r_o,z_o) and the jth element of the time reversal mirror and $N_{j,l}(f)$ is the noise or reverberation. In practice, $\boldsymbol{k}_{jl}(f)$ is replaced by $p(j,l,f)$ to generate the TRO. Since the signal subspace is not completely perpendicular to the noise subspace, the estimation of the transfer function by the eigen-decomposition of the TRO may be not exactly parallel and proportional to the true one.

According to the definition of the inner product of vector, if we use the complex conjugate of the estimated vector as an excitation weight on the time reversal mirror for retransmission, the pressure field of the scatterer can be expressed as

$$p_o(f)=(\hat{\boldsymbol{G}}(f)s(f))^{\boldsymbol{H}}\boldsymbol{G}_n(f)=\frac{\hat{\boldsymbol{G}}^{\boldsymbol{H}}(f)\boldsymbol{G}_n(f)s^*(f)}{\left|\hat{\boldsymbol{G}}(f)\right|\left|\boldsymbol{G}_n(f)\right|}$$
$$=\cos(\hat{\boldsymbol{G}}(f),\boldsymbol{G}_n(f))s^*(f), \quad (5)$$

(the TR is equivalent to a phase conjugation in the frequency domain) where the vectors $\hat{\boldsymbol{G}}(f)$ and $\boldsymbol{G}_n(f)$ are normalized vectors and $\cos(\hat{\boldsymbol{G}}(f),\boldsymbol{G}_n(f))$ is the cosine of the angle between vector $\hat{\boldsymbol{G}}(f)$ and $\boldsymbol{G}_n(f)$. For broadband pulse propagation in a time-reversal mirror, the total signal energy of the field can be obtained using Parseval's relation over the frequency band of the signal:

$$Ps_o=\int_{f_1}^{f_2}\left|p_o(f)\right|^2\mathrm{d}f=\int_{f_1}^{f_2}\left|\cos(\hat{\boldsymbol{G}}(f),\boldsymbol{G}_n(f))\right|^2\left|s(f)\right|^2\mathrm{d}f, \quad (6)$$

where $B=f_2-f_1$ is the signal bandwidth, Ps_o is the signal energy at a certain SNR or signal-to-reverberation ratios (SRR). If the estimated transfer vector is the same as the true one, the total signal energy should be $\int_{f_1}^{f_2}\left|s(f)\right|^2\mathrm{d}f$. Since the noise cannot be ignored, there is an angle between the estimated transfer vector and the correct one. Compared with using the complex conjugate of the true vector as an excitation weight on the time reversal mirror for retransmission, the signal energy that can focus onto the scatterer reduces. The larger the angle is, the more seriously the signal energy reduces. An issue of interest is the side-lobe signal energy in the time-reversal data (Root and Rogers, 2002). Side-lobe signal energy refers to any significant signal energy outside of the focal region. Unfocused signal energy as a function of position can be expressed as

$$P(r,z)=\int_{f_1}^{f_2}\left|\hat{\boldsymbol{G}}^{\boldsymbol{H}}(f)\boldsymbol{G}_n(r,z,f)\right|^2\left|s(f)\right|^2\mathrm{d}f, \quad (7)$$

where $\boldsymbol{G}_n(r,z,f)$ is the normalized Green's function at range r and depth z.

In this study, the performance of the DORT method in a noisy environment is assessed from two aspects. First, we examine the spatial distribution of signal energy at different SNRs or SRRs, and compare the results with the noise-free case (or retransmission weighted by the complex conjugate of the correct transfer vector). To evaluate the spatial focusing and temporal compression, the waveforms of the signals received at different depths along the same range of the retrofocus location are also given. Second, we evaluate the degradation levels (DLs) of the signal

energy at the intended retrofocus location:

$$DL_s = 10\log\frac{Ps_o}{Pi_o}, \tag{8}$$

where and Pi_o is the signal energy in the noise-free case.

SIMULATIONS

In this section, a number of simulations are presented to evaluate the performance degradation of a time reversal mirror in a noise-limited case and in a reverberation-limited case. A Pekeris waveguide is used, whose parameters are ρ_1=1.0×10^3 kg/m^3, c_1=1500 m/s, ρ_2=1.80×10^3 kg/m^3, c_2=1650 m/s, bottom attenuation a_2=0.8 dB/λ and depth D=1.44 m. The SRA is vertical and consists of 32 transducer elements located in range at r=0 m and uniformly in depth from the surface to the bottom. The scatterer locates at r_o=8.5 m and in depth z_o=0.8 m or it lies on the seabed. The transmitted signal is a 4 kHz wideband linear frequency modulated signal with center frequency of 12 kHz. The pulse length of the signal is 1 ms and the sample frequency is 50 kHz. A vertical linear array (VLA) locates at the same range of the scatterer and consists of 33 elements spanning 1.28 m from 0.04 to 1.32 m. The backscattered field used to generate the TRO is computed with KRAKEN. Moreover, the reflection coefficient of the scatterer is simply assumed to be 1 in the bandwidth of the transmitted signal. Each result is obtained by averaging 500 Monte Carlo simulations.

Noise-limited case

In the noise-limited case, the noise $N(f)$ in Eq.(4) is modeled as a stationary homogeneous flat-spectrum band-limited zero-mean Gaussian-distributed noise that is uncorrelated between array elements and between the source and array location. To compare the performance at different SNRs, the power of the retransmitted signals is normalized.

Fig.1 shows spatial focusing in the presence of noise at different SNRs. Although the peak occurs at the intended retrofocus location, the unfocused signal energy increases when the SNR decreases. For example, the signal energy of the side-lobe is only 5 dB less than the main peak when the SNR is −10 dB. Fig.2 shows the degradation of signal energy at the intended retrofocus position as a function of SNR. The signal energy at different SNRs is obtained by the average of the 500 simulations. That is, Ps_o is placed by $E\{Ps_o(n),\ 1\le n\le 500\}$ in Eq.(8). Moreover, the standard deviation is defined as $\sigma=\sqrt{\frac{1}{500-1}\sum_{n=1}^{500}(Ps_o(n)-E\{Ps_o\})^2}$. Fig.2a is similar to Fig.2 of Gaumond *et al.*(2006). Both figures have the same meaning but a different form. This study concerns active focusing in that the retrofocusing performance is evaluated at the target location, while the work of Gaumond *et al.*(2006) concerns passive focusing in that no retransmission is carried out and performance is evaluated at the SRA. In fact, the reason that the signal energy at the intended retrofocus position reduces is that the estimated transfer vector is not accurate. Therefore, the evaluation of the performance degradation at the intended retrofocus position is similar to finding out the accuracy of the resulting mean in estimating the transfer vector at the SRA. Note that the decline is slow when the SNR is higher than 0 dB and the degradation level is less than 2 dB at an SNR of 0 dB. However, the decline is abrupt when the SNR is lower than −2 dB. At the same time, the standard deviation is the highest around −4 dB.

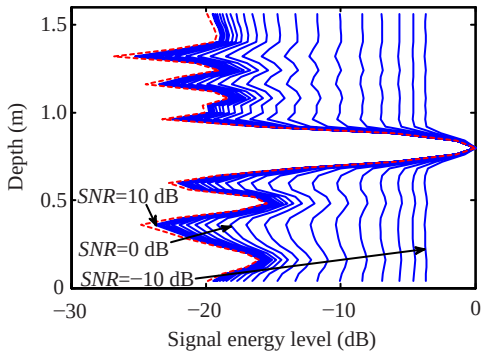

Fig.1 Retrofocused signal energy as a function of depth along the same range as the point scatterer at different SNRs. The dashed line is the criterion of the evaluation that represents the situation without noise. The solid lines from right to left represent the situation in which the SNR becomes higher and higher (from −10 to 10 dB) with increments of 1 dB. The signal energy for each curve is normalized by the peak of its own SNR level

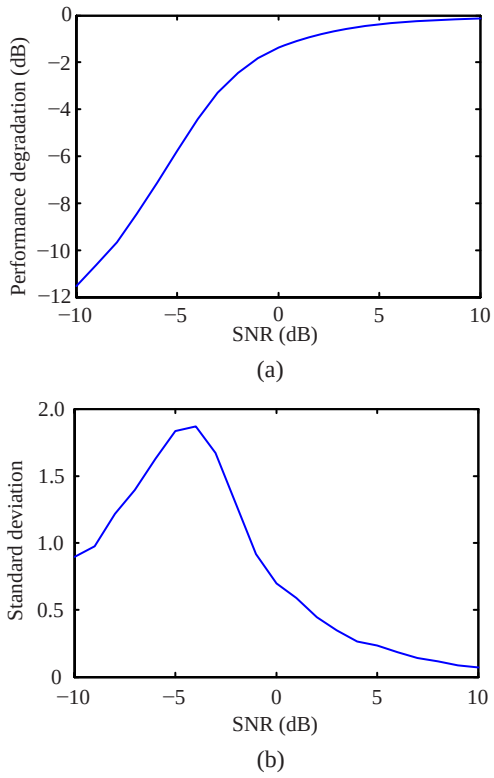

Fig.2 Performance degradation at the intended retrofocus location as a function of SNR in the noise-limited case. (a) The accuracy of the resulting mean; (b) The standard derivation

Fig.3 shows the signal energy in depth versus range coordinates at the SNRs of 0 and −10 dB, which is normalized by the peak signal energy in the noise-free case and converted to decibels. Compared to the noise-free case, the low decibel value of unfocused signal energy in Fig.3a indicates that the vertical side-lobe structure changes little at an SNR of 0 dB. This situation remains true for the SNR slightly below 0 dB. However, at an SNR of −10 dB (Fig.3b), the side-lobe levels are high and the degradation of the signal energy at the intended retrofocus position is serious.

Fig.4 shows the signals received on the VLA which is located at the same range as the scatterer. The scatterer is located at the same depth as element 20 of the VLA. The time series of signals are normalized with respect to their maximum amplitudes. We clearly see a vertical spatial focusing of 0.1 m around the 0.8 m depth (scatterer depth) in Figs.4a and 4b as well as a temporal compression to 1 ms (the original pulse length) in Fig.4d. However, the signal waveform in

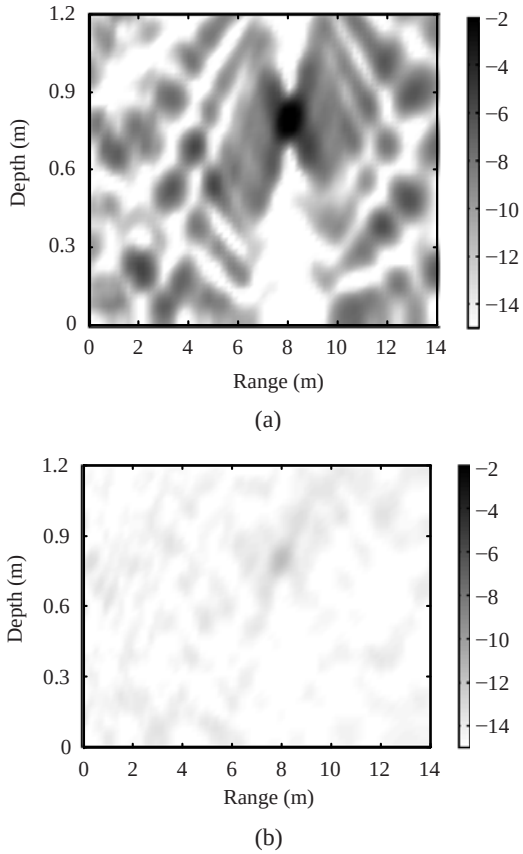

Fig.3 Signal energy in depth versus range coordinates from retransmission weighted by the estimate of the transfer vector, which is normalized by the peak signal energy in the noise-free case and converted to decibels. (a) *SNR*=0 dB; (b) *SNR*=−10 dB

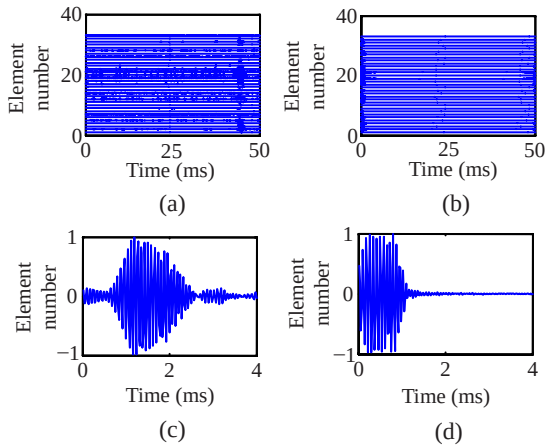

Fig.4 Signals received on the VLA from retransmission (a) weighted by the estimated transfer vector at an *SNR*=0 dB; (b) weighted by the true transfer vector; (c) signal at intended retrofocus location (element 20) extracted from Fig.4a; (d) signal at intended retrofocus location (element 20) extracted from Fig.4b

Fig.4c does not show temporal compression to 1 ms and is different from that of the signal in Fig.4d. The correlation coefficient is 0.76. Moreover, time shift occurs. This is caused by the complex parameter ratio of the estimate transfer vector to the true one (shown in Eq.(3)) due to the random choice of eigenvector for different frequencies. Different singular decomposition methods should be used to improve the focusing capability.

Reverberation-limited case

In a reverberation-limited case, the noise $N(f)$ in Eq.(4) is modeled as in Lingevitch *et al.*(2002) and Song *et al.*(2004). For the purpose of the simulation, it is assumed that the bottom roughness is the dominant contribution to the backscattering. The rough interface realizations are modeled with the 1D Gaussian roughness spectrum (Kuperman and Schmidt, 1989):

$$P(p)=\sqrt{2\pi}L\mathrm{e}^{-p^2L^2/2}, \tag{9}$$

where p is lag ($p=r_1-r_2$) and L=1.25 m is the correlation length of the roughness. Neglecting multiple scattering, roughness in the vicinity of a range r will contribute to the received reverberation over a time window:

$$w(t;r,\Delta)=\begin{cases}1, & \left|t-t_\mathrm{c}-t_0\right|\le\Delta/2,\\ 0, & \left|t-t_\mathrm{c}-t_0\right|>\Delta/2,\end{cases} \tag{10}$$

where $t_\mathrm{c}=2r_\mathrm{o}/c$ is the approximate round-trip travel time and Δ is the width of the temporal window which depends on the source pulse length T and the dispersive properties of the waveguide. Due to dispersion in the waveguide, a span of ranges of width Δr will contribute to the reverberation in the window time series. As in Lingevitch *et al.*(2002) and Song *et al.*(2005), $\Delta=T$ was taken as the time window. The modal representation of the backscattered field at a single frequency (Song *et al.*, 2005) is

$$N(z,z_\mathrm{s},f)=-\frac{1}{8\pi}\sum_n\sum_m\frac{\phi_m(z_\mathrm{s})\phi_m(z_\mathrm{int})b_{mn}\phi_n(z_\mathrm{int})\phi_n(z)}{\sqrt{\kappa_m\kappa_n}}\cdot\int_0^\infty\gamma(r)\mathrm{e}^{-\mathrm{i}(\kappa_m+\kappa_n)r}\mathrm{d}r, \tag{11}$$

where (ϕ_m,κ_m) are the sets of the mth propagating mode and the corresponding horizontal wavenumber, $\gamma(r)$ is the deformation from the unperturbed flat interface z_int, and z_s and z are the depths of the source and receiver, respectively. The modal backscattering strength b_{mn} between modes m and n is:

$$b_{mn}=\left(1-\frac{\rho_\mathrm{b}}{\rho_\mathrm{w}}q_mq_n\right)+\kappa_\mathrm{w}^2-\frac{\rho_\mathrm{w}}{\rho_\mathrm{b}}\kappa_\mathrm{b}^2+\kappa_m\kappa_n\left(1-\frac{\rho_\mathrm{w}}{\rho_\mathrm{b}}\right). \tag{12}$$

where $q_n=\dfrac{\phi_n'(z_\mathrm{int})}{\phi_n(z_\mathrm{int})}=\left(\dfrac{\rho_\mathrm{w}}{\rho_\mathrm{b}}\right)\sqrt{\kappa_n^2-\kappa_\mathrm{b}^2}$. The subscripts w and b denote the water and bottom at the interface $z=z_\mathrm{int}$, respectively, and the prime $'$ indicates a derivation with respect to depth z.

Firstly, a suspended target is considered. Assume that the first eigenvector is used as an excitation weight vector on the time reversal mirror for retransmission to focus the energy on the point-like scatterer. Fig.5 shows the signal energy as a function of depth along the same range as the point scatterer at different SRRs. Unlike in the vertical side-lobe structure in Fig.1, the leakage signal energy mainly focuses on the corresponding bottom interface at an SRR above 0 dB (Fig.5a) while the peak signal energy focuses on the undesirable location at an SRR below 0 dB (Fig.5b). The dual focusing appears especially in the case where the SRR is 0 dB. Provided that reverberation is treated as another point-like scatterer, the reason for the dual focusing can be explained by Prada *et al.*(1996). The case of *SRR*≠0 dB is similar to the situation where the two scatterers' apparent reflectivities are different, while the case of *SRR*=0 dB is similar to the situation where the two scatterers' apparent reflectivities are the same.

In addition, assume that the second eigenvector is used as an excitation weight vector on the time reversal mirror for retransmission. Fig.6 displays the performance degradation at the intended retrofocus location as a function of the SRR. Here, the directivity of the reverberation causes almost no losses to occur when the SRR exceeds 0 dB as well as an abruptly serious degradation at SRR below 0 dB with the first eigenvector weighting the retransmission (Fig.6a). An almost opposite trend is shown in Fig.6b. It is obvious that almost no losses occur in Fig.6a, while there is an

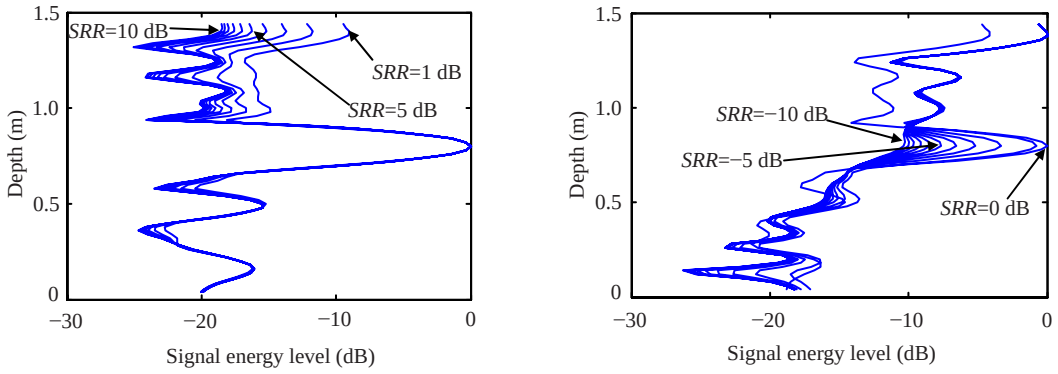

(a) (b)

Fig.5 Retrofocused signal energy as a function of depth along the same range as the point scatterer at different SRRs, which use the first eigenvector to weight the retransmission for a suspended target in a reverberation-limited case. (a) The SRRs are from 1 to 10 dB with increments of 1 dB; (b) The SRRs are from −10 to 0 dB with increments of 1 dB

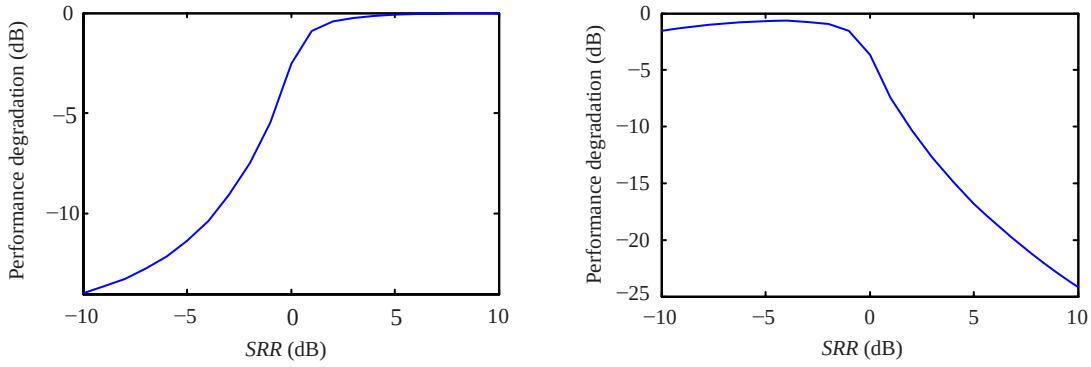

(a) (b)

Fig.6 Performance degradation at the intended retrofocus location as a function of SRR for a suspended target in a reverberation-limited case. (a) Using the first eigenvector to weight the retransmission; (b) Using the second eigenvector to weight the retransmission

abrupt and serious degradation in Fig.6b when the SRR exceeds 0 dB. Similarly, there is an abrupt and serious degradation in Fig.6a while almost no losses occur in Fig.6b when the SRR is below 0 dB. An almost opposite trend is also observed in Fig.7, when compared with that shown in Fig.5. Why does the opposite trend appear? The reason is that the DORT method is a selective detection and focusing technique. If the bottom reverberation is a point-like scatterer, this can be easily understood. Because each scatterer is associated with a certain eigenvector of the time reversal operator, the focusing on one of the scatterers was obtained by transmission with elements weighted by the corresponding eigenvector of the time reversal operator (Prada *et al*., 1996). However, the signal cannot efficiently focus on the target due to a significant secondary lobe at the corresponding bottom interface, which is different from the situation of two point-like scatterers. Moreover, more and more signal energy leaks to the corresponding bottom interface as the SRR decreases, as shown in Fig.5a for SRR above 0 dB. Fig.8 illustrates the retrofocused signal energy in depth versus range coordinates at the SRR of −10 dB with the first and the second eigenvectors as the weight vectors. The figure indicates that the target echo (a point-like scatterer) can be separated from the bottom reverberation (an extended target), although they are not completely separated. Also, as shown in Fig.7a, the wrong choice sometimes causes the opposite result in that the nulls appear at the intended retrofocus location. Therefore, it is important to choose the correct eigenvector to weight the transmission for a suspended target in a reverberation-limited case.

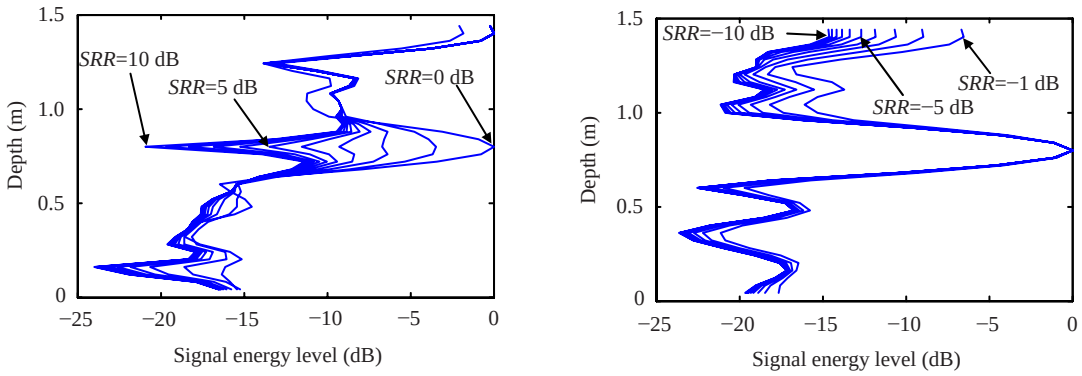

(a) (b)

Fig.7 Retrofocused signal energy as a function of depth along the same range as the point scatterer at different SRRs, using the second eigenvector to weight the retransmission for a suspended target in a reverberation-limited case. (a) The SRRs are from 0 to 10 dB with increments of 1 dB; (b) The SRRs are from −10 to −1 dB with increments of 1 dB

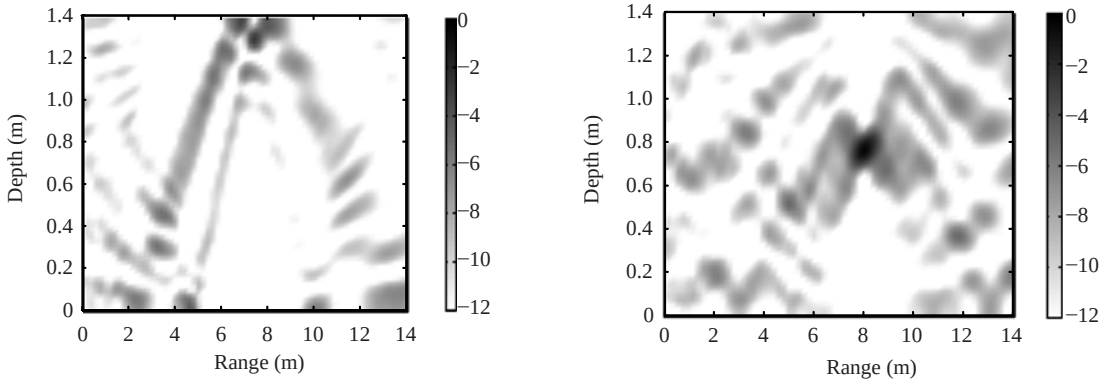

(a) (b)

Fig.8 Retrofocused signal energy in depth versus range coordinates at an SRR of –10 dB for a suspended target in a reverberation-limited case, which is normalized by the retrofocus peak signal energy in the noise-free case and converted to decibels. (a) Using the first eigenvector to weight the retransmission; (b) Using the second eigenvector to weight the retransmission

Secondly, a target placed on the seabed is considered. The first eigenvector is used as an excitation weight vector on the time reversal mirror for retransmission. Fig.9 displays the performance degradation at the intended retrofocus location as a function of SRR. Fig.10 shows the signal energy as a function of depth along the same range as the point-like scatterer at different SRRs. The results show that the losses can almost be neglected even at a low SRR and the performance no longer degrades when the SRR is reduced to a certain extent (e.g., −20 dB in this study). The reason is that stochastic reverberation now plays the main role in guiding the retransmission. The reverberation signals were used to estimate the transfer function between the time reversal mirror and a

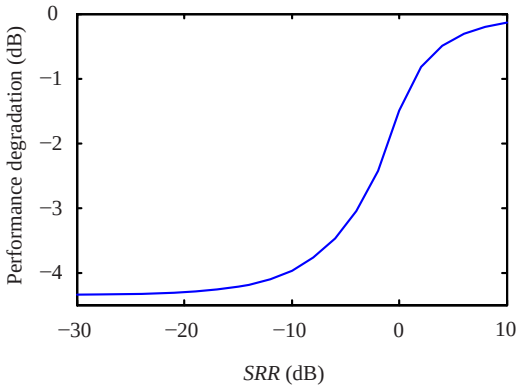

Fig.9 Performance degradation at the intended retrofocus location as a function of SRRs using the first eigenvector to weight the retransmission for a target placed on the bottom in a reverberation-limited case

corresponding range interval on the bottom, and then the estimate of the transfer function was used to focus energy in the vicinity of the water-bottom interface to improve the detection of a target placed on the seabed or buried in the sediments (Sabra *et al*., 2006).

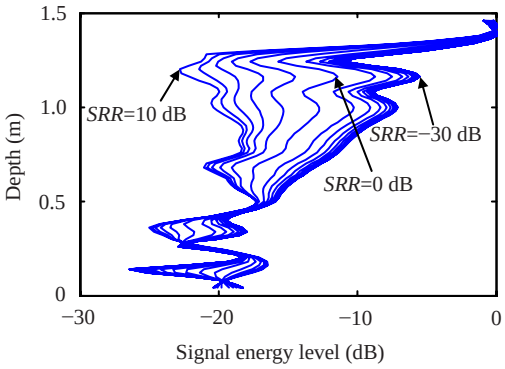

Fig.10 Retrofocused signal energy as a function of depth along the same range as the point scatterer at different SRRs (from −30 to 10 dB) with increments of 2 dB using the first eigenvector to weight the retransmission for a target lying on the seabed in a reverberation-limited case

EXPERIMENTAL RESULTS

This section discusses the focusing performance of DORT at different SNRs or SRRs based on real experimental data.

Laboratory waveguide experiment

The experiment was performed in a laboratory waveguide using a vertical SRA of 32 elements equally spaced at 0.04 m apart. The laboratory waveguide was 14 m in length, 1.2 m in width and 1.44 m in height. Three sides were covered with anechoic tile and the other side was a steel sheet located 13 m away from the SRA. A 0.1 m diameter steel ball suspended at a range of 8.5 m and a depth of 0.80 m was used as a target. The bottom was a steel plate covered with sand of 0.22 m thickness. To produce strong reverberation, a stack of pebbles was heaped up at the bottom with the same range as the target. The transmitted signal was a T=1 ms linear frequency modulated (LFM) signal with a center frequency of 12 kHz and 4 kHz bandwidth.

The experiments were conducted as follows:

(1) Without the target being placed in the waveguide, a transmission with a probing beam, via a forward model which provided a transfer function between the SRA and the corresponding range interval on the bottom, was used to produce a strong reverberation return (Li J.L. *et al*., 2008).

(2) Select time-gated portion of the reverberation signal $\boldsymbol{R}_m(t_c+t_o-\Delta/2\le t\le t_c+t_o+\Delta/2)$, $1\le m\le M$ (M is the number of snapshots). Thereby, the reverberation data were obtained. Multiple snapshots were collected from the same beam to construct a data correlation matrix.

(3) With a target placed in the waveguide, the echo return levels were maximized using a probing beam of different source levels (SL_q, $1\le q\le Q$, Q is the number of source levels) ensonifying the target.

(4) The same processing was used to obtain the echo data $\boldsymbol{Ec}_{mq}(t_c+t_o-\Delta/2\le t\le t_c+t_o+\Delta/2)$, $1\le m\le M$. Multiple snapshots were collected from the same beam to construct a data correlation matrix.

(5) At the end, a segment of acoustic noise was recorded. Select random portion of noise $\boldsymbol{N}(t_m-\Delta/2\le t\le t_m+\Delta/2)$, $1\le m\le M$, with the same length as that of the echo data.

Processing results

To obtain noisy backscattered signals at different SNRs, we add amplified acoustic noises to the echoes of the target. The SNR is defined by

$$SNR_q=\frac{\frac{1}{M}\sum_{m=1}^{M}\int_{-\Delta/2}^{\Delta/2}\left|\boldsymbol{Ec}_{mq}(t_c+t_0+t)\right|^2\mathrm{d}t}{\frac{1}{M}\sum_{m=1}^{M}\int_{-\Delta/2}^{\Delta/2}\left|A\boldsymbol{N}(t_m+t)\right|^2\mathrm{d}t},\qquad(13)$$

where A=30 and M=3. Different SNR levels were met by different source levels.

At the qth transmission, assume that the backscattered signal received is $\boldsymbol{Sb}_m(t)=\boldsymbol{Ec}_{mq}(t_c+t_o-\Delta/2\le t\le t_c+t_o+\Delta/2)+A\boldsymbol{N}(t_m-\Delta/2\le t\le t_m+\Delta/2)$. A Fourier transform is applied and $\boldsymbol{Sb}_m(f)$ can be obtained. The TRO can be approximated by $\boldsymbol{K}^H(f)\boldsymbol{K}(f)=\sum_{m=1}^{M}\boldsymbol{Sb}_m(f)\boldsymbol{Sb}_m^H(f)$ (Song *et al*., 2005). Therefore, we can obtain the TRO at different SNRs.

Fig.11 shows the corresponding experimental result, almost in agreement with the simulated result shown in Fig.1. It also shows that the focusing cannot be achieved when the SNR is below −10 dB. The reason that the energies fluctuate (except for the

intended retrofocus location) is that the experimental results were obtained at only one time while the simulated results were obtained by averaging 500 Monte Carlo simulations.

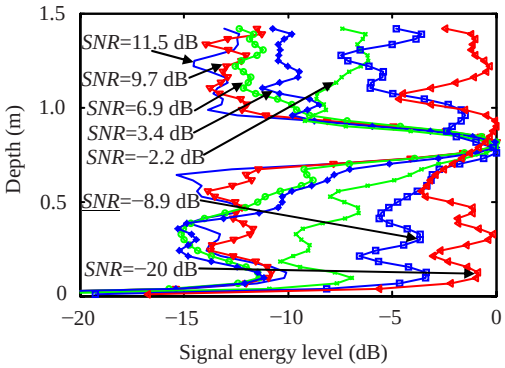

Fig.11 Retrofocused signal energy as a function of depth along the same range as the point scatterer at different SNRs using real experimental data. The signal energy for each curve is normalized by the peak of its own SNR level

Similarly, the SRR is defined by

$$SRR_q = \frac{\frac{1}{M}\sum_{m=1}^{M}\int_{-\Delta/2}^{\Delta/2}\left|\boldsymbol{Ec}_{mq}(t_c+t_0+t)\right|^2 \mathrm{d}t}{\frac{1}{M}\sum_{m=1}^{M}\int_{-\Delta/2}^{\Delta/2}\left|\boldsymbol{R}_m(t_c+t_0+t)\right|^2 \mathrm{d}t}. \quad (14)$$

In fact, the SNR and SRR computed as above, are a bit higher than the real ones especially for the lower source level, because there are some noises or reverberations in the echoes. It is impossible for the laboratory waveguide environment to be as exact as the simulation. For example, an anechoic tile cannot absorb sound completely, and the response of the SRA element is not exact.

Similarly, we obtained the TRO at different SRRs.

Figs.12 and 13 show the corresponding experimental results, almost in agreement with the simulated results shown in Fig.5 and Fig.7b.

CONCLUSION

In this study we presented the results of theoretical, simulation and experimental investigations on performance degradation using the DORT method

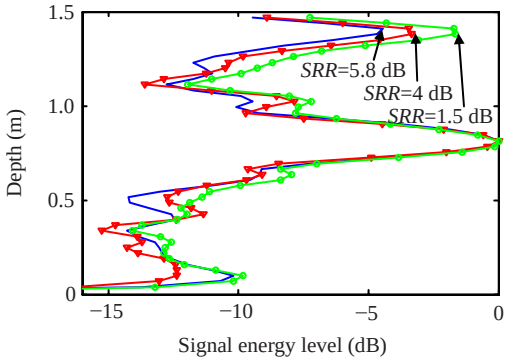

(a)

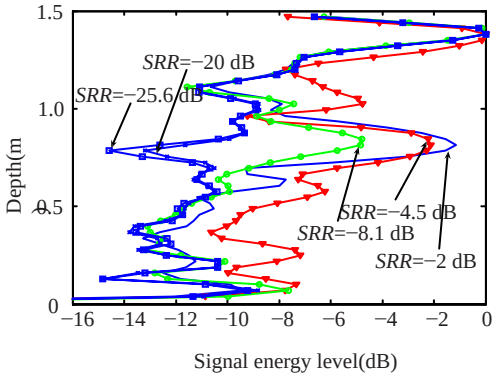

(b)

Fig.12 Retrofocused signal energy as a function of depth along the same range as the point scatterer at different SRRs, using the first eigenvector to weight the retransmission for a suspended target in a reverberation-limited case using real experimental data. (a) The SRRs are higher than 0 dB; (b) The SRRs are lower than 0 dB

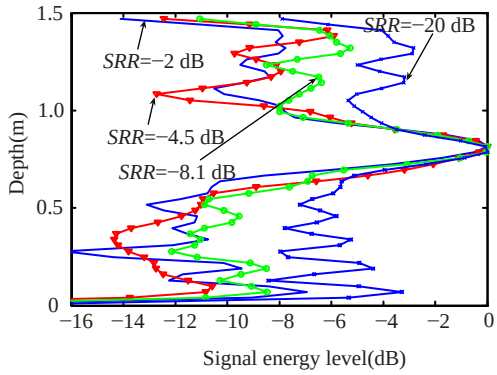

Fig.13 Retrofocused signal energy as a function of depth along the same range as the point scatterer at different SRRs (below 0 dB), using the second eigenvector to weight the retransmission for a suspended target in a reverberation-limited case using real experimental data

in noisy environments with broadband signals. The main purpose was to assess the application of the DORT in noise-limited and in reverberation-limited cases.

In a noise-limited case, there is not a significant secondary lobe because the unfocused signal energy is almost uniformly distributed. Besides, unfocused signal energy increases as the SNR decreases. The peak signal energy focuses on the intended location, so the DORT method can exert its focusing function even in a noise-limited case. This can be explained as follows: the time reversal method can take the advantage of multi-path propagation in waveguide environments. The weight vector for the retransmission is matched to the channel.

However, it is quite different in a reverberation-limited situation. A secondary lobe appears at the position of reverberation. The performance degradation may be small even at a lower SRR if a proper eigenvector is chosen for a suspended target. For a target placed on the bottom, the performance degradation is smaller than that for the suspended target and can be neglected. However, this does not mean that it is beneficial to target detection on the bottom. The disadvantage is that the point-like scatterer and the bottom reverberation cannot be resolved any more because the source array is not able to focus sound on the scatterer independently with a beam. This implies that the echo-to-reverberation ratio cannot be enhanced even if the signal energy focuses on the target. When the SRR decreases to a certain extent (for example, −20 dB in this research), the reverberation plays the main role in focusing signal energy on the seabed interface co-located with the scatterer.

Overall, because it is more difficult to separate the target echo from noise than from the reverberation for a suspended target, the DORT method can be efficiently applied for target detection with a sufficient source level to yield significant backscatter. Generally, the backscattered signal energy measured in a monostatic configuration is dominated by ocean bottom reverberation for shallow water waveguides. Therefore, the DORT is a promising technology for active target detection in unknown shallow water environments. However, how to distinguish a target echo with constant backscattering return from strong local clutter on the bottom (false alarms) needs to be solved in the future if the DORT is to be applied in detecting targets which are placed on the bottom in reverberation-limited situations.

References

Carin, L., Liu, H.W., Yoder, T., Couchman, L., Houston, B., Bucoro, J., 2004. Wideband time-reversal imaging of an elastic target in an acoustic waveguide. *J. Acoust. Soc. Am.*, **115**(1):259-268. [doi:10.1121/1.1632482]

Folegot, T., Prada, C., Fink, M., 2003. Resolution enhancement and separation of reverberation from target echo with the time reversal operator decomposition. *J. Acoust. Soc. Am.*, **113**(6):3155-3160. [doi:10.1121/1.1571541]

Gaumond, C.F., David, M.F., Lingevitch, J.F., Menis, R., Edelmann, G.F., Calvo, D.C., Kim, E., 2006. Demonstration at sea of the decomposition-of-the-time-reversal-operator technique. *J. Acoust. Soc. Am.*, **119**(2):976-990. [doi:10.1121/1.2150152]

Jackson, D.R., Dowling, D.R., 1991. Phase conjugation in underwater acoustics. *J. Acoust. Soc. Am.*, **89**(1):171-181. [doi:10.1121/1.400496]

Kim, S., Kuperman, W.A., Hodgkiss, W.S., Song, H.C., Edelmann, G., Akal, T., 2004. Echo-to-reverberation enhancement using a time reversal mirror. *J. Acoust. Soc. Am.*, **115**(4):1525-1531. [doi:10.1121/1.1649737]

Kuperman, W.A., Schmidt, H., 1989. Self-consistent perturbation approach to rough surface scattering in stratified elastic media. *J. Acoust. Soc. Am.*, **86**(4):1511-1522. [doi:10.1121/1.398712]

Kuperman, W.A., Hodgkiss, W.S., Song, H.C., Akal, T., Ferla, C., Jackson, D.R., 1998. Phase conjugation in the ocean: Experimental demonstration of an acoustic time-reversal mirror. *J. Acoust. Soc. Am.*, **103**(1):25-40. [doi:10.1121/1.423233]

Li, C.X., Gong, X.Y., Zou, L.N., 2008. Decomposition and retrofocusing performance of the time reversal operator of narrowband signal without interference. *J. Harbin Eng. Univ.*, **29**(8):867-871(in Chinese).

Li, J.L., Pan, X., Yan, L.M., Zhao, H.F., 2008. Buried Target Detection Based on Time Reversal by Probing Beam. OCEANS MTS/IEEE, KOBE, Japan, p.293-298.

Lingevitch, J.F., Song, H.C., Kuperman, W.A., 2002. Time reversed reverberation focusing in a waveguide. *J. Acoust. Soc. Am.*, **111**(6):2609-2614. [doi:10.1121/1.1479148]

Prada, C., Thomas, J.L., Fink, M., 1995. The iterative time reversal process: Analysis of the convergence. *J. Acoust. Soc. Am.*, **97**(1):62-71. [doi:10.1121/1.412285]

Prada, C., Manneville, D., Spoliansky, D., Fink, M., 1996. Decomposition of the time reversal operator: Detection and selective focusing on two scatterers. *J. Acoust. Soc. Am.*, **99**(4):2067-2076. [doi:10.1121/1.415393]

Root, J.A., Rogers, P.H., 2002. Performance of an underwater acoustic volume array using time-reversal focusing. *J. Acoust. Soc. Am.*, **112**(5):1869-1878. [doi:10.1121/1.1509073]

Roux, P., Fink, M., 2000. Time reversal in a waveguide: Study of the temporal and spatial focusing. *J. Acoust. Soc. Am.*,

107(5):2418-2429. [doi:10.1121/1.428628]

Sabra, K.G., Khosla, S.R., Dowling, D.R., 2002. Broadband time-reversal array retrofocusing in noisy environments. *J. Acoust. Soc. Am.*, **111**(2):823-830. [doi:10.1121/1.1432984]

Sabra, K.G., Roux, P., Song, H.C., Hodgkiss, W.S., Kuperman, W.A., Akal, T., Stevenson, J.M., 2006. Experimental demonstration of iterative time-reversal reverberation focusing in a rough waveguide. Application to target detection. *J. Acoust. Soc. Am.*, **120**(3):1305-1314.

Song, H.C., Kuperman, W.A., Hodgkiss, W.S., 1998. A time-reversal mirror with variable range focusing. *J. Acoust. Soc. Am.*, **103**(6):3234-3240. [doi:10.1121/1.423040]

Song, H.C., Kuperman, W.A., Hondgkiss, W.S., Akal, T., Ferla, C., 1999. Iterative time reversal in the ocean. *J. Acoust. Soc. Am.*, **105**(6):3176-3184. [doi:10.1121/1.424648]

Song, H.C., Kim, S., Hodgkiss, W.S., Kuperman, W.A., 2004. Environmentally adaptive reverberation nulling using a time reversal mirror. *J. Acoust. Soc.Am.*, **116**(2):762-768. [doi:10.1121/1.1765194]

Song, H.C., Hodgkiss, W.S., Kuperman, W.A., Roux, P., Akal, T., Stevenson, M., 2005. Experimental demonstration of adaptive reverberation nulling using time reversal. *J. Acoust. Soc. Am.*, **118**(3):1381-1387. [doi:10.1121/1.1984990]

Walker, S.C., Philippe, R., Kuperman, W.A., 2005. Focal depth shifting of a time reversal mirror in a range-independent waveguide. *J. Acoust. Soc. Am.*, **118**(3):1341-1347. [doi:10.1121/1.1940447]

Walker, S.C., Kuperman, W.A., Roux, P., 2006. Active waveguide Green's function estimation with application to time-reversal focusing without a probe source in a range-independent waveguide. *J. Acoust. Soc. Am.*, **120**(5):2755-2763. [doi:10.1121/1.2355538]